

Radial Distribution Function in a Two Dimensional Core-Shoulder Particle System

Michael Wassermair^{1,2,3,*}, Gerhard Kahl^{1,†}, Andrew J. Archer^{2,‡} and Roland Roth^{4,§}

¹*Institut für Theoretische Physik, TU Wien,*

Wiedner Hauptstraße 8-10, A-1040 Vienna, Austria

²*Department of Mathematical Sciences and Interdisciplinary*

Centre for Mathematical Modelling, Loughborough University,

Loughborough LE11 3TU, United Kingdom

³*Institute of Science and Technology Austria,*

A-3400 Klosterneuburg, Austria and

⁴*Institute for Theoretical Physics, University of Tübingen, D-72076 Tübingen, Germany*

(Dated: March 26, 2026)

Abstract

An important quantity in liquid state theory is the radial distribution function $g(r)$. It can be calculated within the framework of classical density functional theory in two very distinct ways. In the test-particle route, one fixes a single fluid particle, turning it into an external potential in which the inhomogeneous structure of the fluid is calculated by minimising the functional. The second route to $g(r)$ in density functional theory employs the Ornstein-Zernike equation and the pair direct correlation function, that can be obtained from the second functional derivatives of the excess free energy functional. Since typically an approximate excess free energy functional is employed, one generally expects that the test-particle route, which requires only one functional derivative, to be more accurate than the Ornstein-Zernike route. Here we study a two dimensional core-shoulder particle system and present results that challenge this expectation. Our results show that in this system test-particle results for $g(r)$ are not always better than results obtained via the Ornstein-Zernike route.

* Michael.Wassermair@ist.ac.at

† Gerhard.Kahl@tuwien.ac.at

‡ A.J.Archer@lboro.ac.uk

§ corresponding author; Roland.Roth@uni-tuebingen.de

I. INTRODUCTION

The radial distribution function (RDF) $g(r)$ of a simple fluid characterises the local structure and correlations between particles and is an important quantity in liquid state theory [1]. It establishes a bridge between the microscopic description of a fluid and macroscopic quantities such as the internal energy, the pressure or the static structure factor of the fluid (see, e.g., Ref. [1]). The function $g(r)$ measures the likelihood of finding a particle at distance r from a *test* particle, relative to that in an ideal gas. For small separations r the structure of $g(r)$ is strongly influenced by the particle-particle interaction. For fluids with a hard core of diameter $\sigma = 2R$, like the fluid we study here, $g(r)$ displays a so-called correlation hole, which implies $g(r \leq \sigma) \equiv 0$. The correlation hole is followed by the first correlation shell of roughly one particle diameter width, that contains information about the nearest neighbours of the test particle, followed by the second correlation shell and so on. Eventually for large distance $r \rightarrow \infty$ particles are randomly placed relative to the test particle, like in the case of an ideal gas, and so as $r \rightarrow \infty$, $g(r) \rightarrow 1$. For short-ranged potentials, like the hard core shoulder potential employed in the present study, the decay of the radial distribution function is exponential and the decay length is the correlation length [1, 2]. Because of the importance of $g(r)$ and the quantities that can be derived from it, there are many different approaches to compute this function, including classical density functional theory (DFT) [1, 3, 4], integral equation theory that combines the Ornstein-Zernike (OZ) equation [5] with a closure relation [1], and computer simulations [6].

In this manuscript we employ DFT to study $g(r)$ for a hard core square-shoulder fluid in two dimensions with an interaction potential that is given by

$$\phi(r) = \begin{cases} \infty & r \leq \sigma, \\ \epsilon & \sigma < r < \lambda\sigma, \\ 0 & \lambda\sigma \leq r, \end{cases} \quad (1)$$

where $\lambda\sigma$ is the range of the (repulsive) square-shoulder interaction with a height $\epsilon > 0$. Within DFT one can prove [1, 3, 4] that there exists the grand potential functional $\Omega[\rho(\mathbf{r})]$, that it is a functional of the ensemble averaged one-particle density $\rho(\mathbf{r})$, and that it is minimised by the equilibrium density distribution $\rho_0(\mathbf{r})$, for which the functional reduces to the grand potential $\Omega = \Omega[\rho_0(\mathbf{r})]$ of the system. This can be written in the compact form of

the Euler-Lagrange equation [4]

$$\left. \frac{\delta\Omega[\rho]}{\delta\rho(\mathbf{r})} \right|_{\rho(\mathbf{r})=\rho_0(\mathbf{r})} = 0. \quad (2)$$

Unfortunately, the mathematical proof of DFT, that guarantees the existence of the functional does not provide insight in how the functional, especially the part that describes inter-particle interaction, is constructed. Several approximations for hard spheres in dimension $d = 3$ have been found [7–9], the most successful being fundamental measure theory (FMT) [9, 10]. FMT follows the structure of the exact DFT for hard rods in $d = 1$ [11, 12], which makes use of the geometrical measures of the particle shapes to account for the hard core repulsion. FMT functionals [9, 13–16] provide a very accurate description of hard sphere fluids compared to computer simulations. The ideas of FMT have been successfully transferred [17, 18] and applied to hard disk fluids in $d = 2$ [19]. Within the framework of DFT the soft (finite) part of the inter-particle interaction in Eq. (1), is typically treated by a random phase approximation (RPA) [1, 20].

DFT offers two very distinct routes to calculate $g(r)$. The first approach is called the test-particle route and was suggested by Percus [21, 22], who realised that a particle of the fluid can be fixed at e.g. the origin of our coordinate system and thereby be made an external potential acting on the rest of the fluid. The external potential $V_{\text{ext}}(r) = \phi(r)$ is the pair potential of the fluid, which in the present case is radially symmetric. If one minimises the density functional to obtain the equilibrium density profile $\rho(r)$ in this external potential, it is related to the radial distribution function via $g(r) = \rho(r)/\rho_b$, where ρ_b is the bulk density far away from the test particle. This approach requires one to only take one functional derivative of the *approximate* grand potential functional $\Omega[\rho]$ in order to calculate the Euler-Lagrange equation, Eq. (2), which can be solved numerically using e.g. a Picard iteration.

The second approach makes use of the OZ relation, which connects the total correlation function $h(r) = g(r) - 1$ with the so-called pair direct correlation function (pDCF) $c^{(2)}(r)$ via [1, 5]

$$h(r) = c^{(2)}(r) + \rho_b \int c^{(2)}(|\mathbf{r} - \mathbf{r}'|)h(r')d\mathbf{r}'. \quad (3)$$

In order to solve this equation an additional closure relation which relates the functions $h(r)$ and $c^{(2)}(r)$ is required. However, within DFT it is possible to calculate the pDCF $c^{(2)}(r)$

from the excess free energy functional $F_{\text{ex}}[\rho(\mathbf{r})]$ [4]

$$c^{(2)}(r = |\mathbf{r} - \mathbf{r}'|) = -\beta \frac{\delta^2 F_{\text{ex}}[\rho(\mathbf{r})]}{\delta\rho(\mathbf{r})\delta\rho(\mathbf{r}')}, \quad (4)$$

which requires the second functional derivative of the *approximate* density functional. From a FMT functional it is possible to obtain a closed analytical expression for the pDCF, which can be employed to solve the OZ equation, i.e. the approximate excess free energy functional $F_{\text{ex}}[\rho(\mathbf{r})]$ replaces the need for an additional (approximate) closure relation.

The core condition $g(r \leq \sigma) \equiv 0$ for hard cores is often part of a closure relation [1, 23], but is usually violated when a pDCF obtained via Eq. (4) is employed in the OZ equation [24]. This is acceptable as long as the RDF outside of the core is accurate. Within DFT the typical experience is that $g(r)$ predicted by the test-particle route is more accurate than the one obtained via the pDCF. The explanation or rationalisation for this comes from the fact that a computation that requires only one functional derivative of an approximate functional should be more reliable than one that requires two functional derivatives. Another rationalisation is the one discussed in [20], based on the observation that the test-particle Euler-Lagrange equation can be written in the form of the OZ equation, that turns out to have a hybrid closure relation that is better than one might expect from just considering Eq. (4). We discuss this issue in more detail in Appendix A of this paper. However, in contrast to the expectations based on these kinds of arguments, here we present results which challenge these expectations about the relative accuracy of the test-particle versus OZ routes to $g(r)$.

In this manuscript we employ DFT for a two dimensional hard core square-shoulder fluid [25, 26] in order to predict the RDF $g(r)$ using the test-particle route and compare these results to $g(r)$ obtained via the OZ equation together with a pDCF obtained from the same density functional. The manuscript is structured as follows. We present the theory in Sec. II, where we specify the details of the density functional employed here, give details about the Monte-Carlo simulation approach used for obtaining benchmark $g(r)$ data and other details relating to how we perform the calculations. In Sec. III we present our results. In Sec. IV we discuss the findings and possible implications of our investigations. In Appendix A we briefly discuss how the OZ equation in combination with the random phase approximation (RPA) closure relates to the RPA-DFT Euler-Lagrange equation in the test-particle limit, while in Appendix B we give a few of the technical details relating to our DFT calculations.

II. THEORY

We consider a two dimensional one-component fluid with pair interactions between the particles, within the framework of DFT. The grand potential functional is given by [1, 4]

$$\Omega[\rho] = F_{\text{id}}[\rho] + F_{\text{ex}}[\rho] + \int \rho(\mathbf{r}) [V_{\text{ext}}(\mathbf{r}) - \mu] d\mathbf{r}, \quad (5)$$

where μ is the chemical potential and $V_{\text{ext}}(\mathbf{r})$ is the external potential. The ideal gas contribution to the free energy in two dimensions $F_{\text{id}}[\rho]$ is known exactly and is given by

$$F_{\text{id}}[\rho] = k_{\text{B}}T \int \rho(\mathbf{r}) [\ln \Lambda^2 \rho(\mathbf{r}) - 1] d\mathbf{r}, \quad (6)$$

with the thermal de Broglie wavelength Λ . The excess (over the ideal gas) Helmholtz free energy functional $F_{\text{ex}}[\rho]$, which contains all the information about the inter-particle interaction, can be decomposed, within perturbation theory, into two contributions

$$F_{\text{ex}}[\rho] = F_{\text{c}}[\rho] + F_{\text{sh}}[\rho]. \quad (7)$$

The first term incorporates the contribution due to the hard core particle interactions and represents the reference system for the fluid with the interaction given in Eq. (1). It is approximated within fundamental measure theory (FMT) [9, 10, 18, 25], which makes the ansatz that the excess free energy functional is a volume integral of an excess free energy density, that is a function of position-dependent weighted densities. For a fluid of hard disks the related state of the art functional is given by [18]

$$F_{\text{c}}^{\text{FMT}}[\rho] = k_{\text{B}}T \int \left[-n_0(\mathbf{r}) \ln(1 - n_2(\mathbf{r})) + \frac{1}{4\pi(1 - n_2(\mathbf{r}))} \left(\frac{19}{12}(\mathbf{n}^{(0)}(\mathbf{r}))^2 - \frac{5}{12}\mathbf{n}^{(1)}(\mathbf{r}) \cdot \mathbf{n}^{(1)}(\mathbf{r}) - \frac{7}{6}\mathbf{n}^{(2)}(\mathbf{r}) \cdot \mathbf{n}^{(2)}(\mathbf{r}) \right) \right] d\mathbf{r}, \quad (8)$$

with weighted densities $n_{\alpha}(\mathbf{r})$ (with $\alpha = 0, 2$) and $\mathbf{n}^{(m)}(\mathbf{r})$ (with $m = 0, 1, 2$) that are convolutions of the local density $\rho(\mathbf{r})$ with geometrical weight functions $\omega_{\alpha}(\mathbf{r})$ and $\omega^{(m)}(\mathbf{r})$. For hard disks one requires two scalar weighted densities

$$n_{\alpha}(\mathbf{r}) = [\rho \otimes \omega_{\alpha}](\mathbf{r}), \quad \alpha = 0, 2, \quad (9)$$

and three tensorial weighted densities

$$\mathbf{n}^{(m)}(\mathbf{r}) = [\rho \otimes \omega^{(m)}](\mathbf{r}), \quad m = 0, 1, 2. \quad (10)$$

The weight functions are [18]

$$\omega_0(r) = \frac{\delta(R-r)}{2\pi R} \quad \text{and} \quad \omega_2(r) = \Theta(R-r), \quad (11)$$

where $R = \sigma/2$ is the radius of the disks, $\delta(r)$ is the Dirac delta distribution and $\Theta(r)$ is the Heaviside step-function. The tensorial weight functions are given by

$$\omega^{(m)}(\mathbf{r}) = \delta(R - |\mathbf{r}|) \underbrace{\hat{\mathbf{r}} \dots \hat{\mathbf{r}}}_{m\text{-times}}. \quad (12)$$

The rank m tensorial weight function arises from taking m tensor products of the unit vector $\hat{\mathbf{r}}$ with itself.

The second term in Eq. (7) is the following RPA approximation [1, 4, 20, 25]

$$F_{\text{sh}}[\rho] = \frac{1}{2} \int \int \rho(\mathbf{r})\rho(\mathbf{r}')\phi_{\text{sh}}(|\mathbf{r} - \mathbf{r}'|)d\mathbf{r}d\mathbf{r}', \quad (13)$$

where

$$\phi_{\text{sh}}(r) = \begin{cases} \epsilon & 0 < r < \lambda\sigma, \\ 0 & \lambda\sigma \leq r, \end{cases} \quad (14)$$

is the repulsive shoulder part of the pair potential. Note that the repulsion has been extended inside the core of the particles.

Having fully specified the excess free energy functional, we are in the position to compute the pDCF using Eq. (4). Since the OZ equation, Eq. (3), can most easily be solved in Fourier space to give

$$\hat{h}(k) = \frac{\hat{c}^{(2)}(k)}{1 - \rho \hat{c}^{(2)}(k)}, \quad (15)$$

we require the Fourier transform of the pDCF $\hat{c}^{(2)}(k)$. Note that the functional form of the excess free energy functional given in (7) implies that the pDCF, within perturbation theory, can be split into two terms, which obviously also holds for its Fourier transform

$$\hat{c}^{(2)}(k) = \hat{c}_c^{(2)}(k) + \hat{c}_{\text{sh}}^{(2)}(k). \quad (16)$$

The first term, arising from the hard disk core repulsion treated using Eq. (8), makes use of the structure of FMT. One finds that the core contribution to the pDCF, Eq. (4) can be written as

$$c_c^{(2)}(r = |\mathbf{r}_1 - \mathbf{r}_2|) = - \sum_{\alpha, \gamma} \frac{\partial^2 \Phi}{\partial n_\alpha \partial n_\gamma} \int d\mathbf{r}' \omega_\alpha(\mathbf{r}' - \mathbf{r}_1) \omega_\gamma(\mathbf{r}' - \mathbf{r}_2), \quad (17)$$

where Φ is the integrand in Eq. (8). Equation (17) can be transformed into Fourier space with the help of the convolution theorem, giving

$$\hat{c}_c^{(2)}(k) = - \sum_{\alpha, \gamma} \frac{\partial^2 \Phi}{\partial n_\alpha \partial n_\gamma} \omega_\alpha(k) \omega_\gamma(-k). \quad (18)$$

The second derivatives of Φ w.r.t. the weighted densities and the Fourier transforms of the weight functions are known analytically and hence we arrive at the following analytical expression for $\hat{c}_c^{(2)}(k)$ [19, 25]

$$\begin{aligned} \hat{c}_c^{(2)}(k) = \frac{\pi}{6(1-\eta)^3 k^2} & \left[-\frac{5}{4}(1-\eta)^2 k^2 J_0(k/2)^2 \right. \\ & + \left(4((\eta-20)\eta+7) + \frac{5}{4}(1-\eta)^2 k^2 \right) J_1(k/2)^2 \\ & \left. + 2(\eta-13)(1-\eta)k J_1(k/2) J_0(k/2) \right], \quad (19) \end{aligned}$$

where $J_n(x)$ are Bessel functions of order n . The second term in Eq. (16) is the contribution from the shoulder to the pDCF, generated by the functional in Eq. (13), and may be written as [25]

$$\hat{c}_{\text{sh}}^{(2)}(k) = -\beta 2\pi\epsilon\lambda \frac{J_1(\lambda k)}{k}. \quad (20)$$

With the explicit expression for $\hat{c}^{(2)}(k)$, the total correlation function $h(r)$ can be calculated via an inverse Fourier transform.

As benchmark data for our DFT results we perform grand canonical Monte-Carlo (GCMC) simulation of the square-shoulder system, to obtain $g(r)$. The GCMC simulations for the liquids were performed in square boxes of size $125\sigma \times 125\sigma$. A total of 20×10^9 GCMC-moves was performed, where in each step particle translation, creation and deletion was attempted with equal probability $\alpha_t = \alpha_c = \alpha_d = \frac{1}{3}$. For the densities considered the simulations contained roughly 2000-8000 particles. The RDF is calculated from the positions of the particles, \mathbf{r}_i via [1]

$$g(r) = \frac{1}{\rho_b} \left\langle \frac{1}{N} \sum_{i=1}^N \sum_{j=1, j \neq i}^N \delta(\mathbf{r} + \mathbf{r}_i - \mathbf{r}_j) \right\rangle, \quad (21)$$

where the brackets denote a grand-canonical average. This ensemble average was performed over 250 configurations, which were separated by 20×10^6 MC-moves along a Markov-chain.

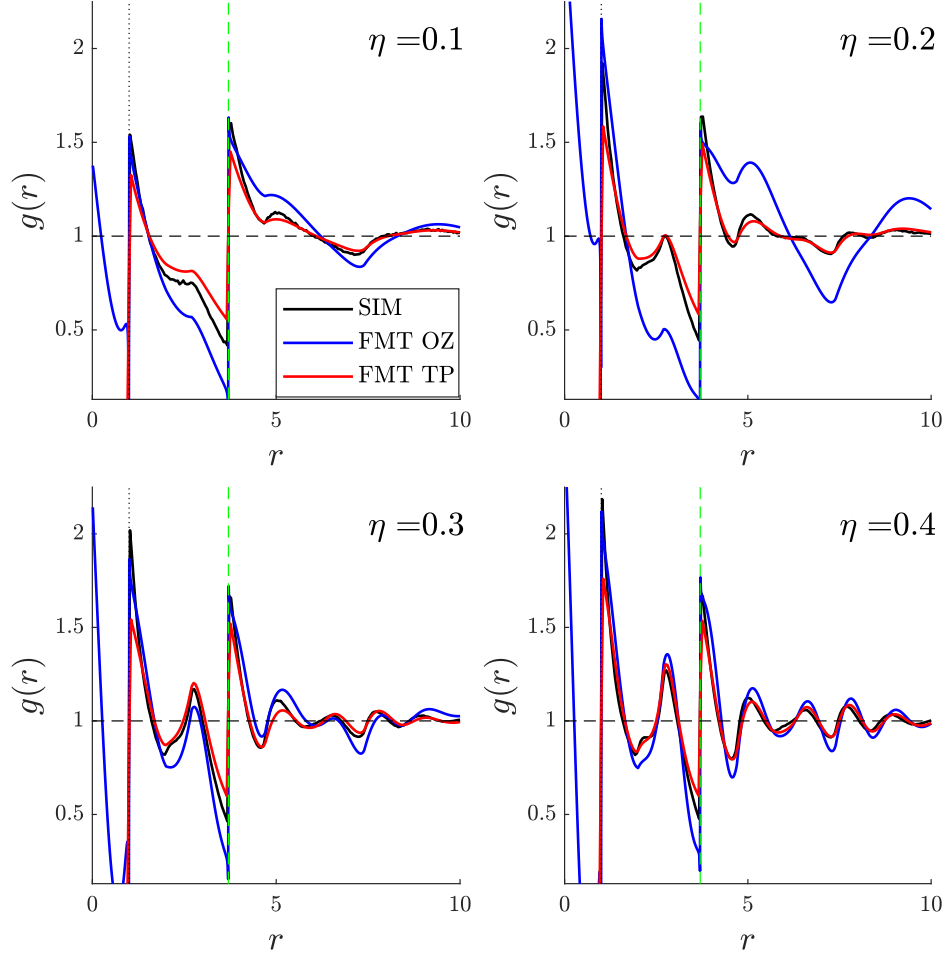


FIG. 1: RDF $g(r)$ as obtained from the Ornstein-Zernike (OZ) route (blue lines), the test-particle (TP) route (red lines) and from GCMC simulations (black lines) for $\lambda = 3.7$ and $T = 0.7402$ and η -values as labelled. For this value of λ we find that the results from the test-particle route agree better with the simulation results than those from the Ornstein-Zernike route.

III. RESULTS

In following we make use of some reduced units. We set the hard disk diameter $\sigma = 1$ as the unit of length and hence measure all other length in units of σ . The temperature T of the system sets an energy scale $k_B T$, where k_B is the Boltzmann constant. In the present problem the only other energy scale that can be compared to $k_B T$ is the shoulder height ϵ in Eq. (1), which enters our calculation as the dimensionless quantity $\beta\epsilon$, where $\beta = 1/(k_B T)$, as usual. To change the temperature in our system we *effectively* set $\beta \equiv 1$ and use, following our previous convention [25], $T = 1/\epsilon$. In this study we want to stay in the fluid phase.

We report results for two different values of the interaction range, $\lambda = 3.7$ and 4.9 , and start with $\lambda = 3.7$. These rather large values of the square-shoulder range give rise to interesting crystalline and quasi-crystalline behaviour at low temperature [26]. First we study the RDF $g(r)$ using the test-particle approach. In order to do so we have to fix one particle at the origin and turn it into an external potential for the rest of the system. The external potential is set to be equal to the pair potential, $V_{\text{ext}}(\mathbf{r}) = \phi(r)$. It might seem best to make use of the radial symmetry of the problem and reduce the resulting DFT calculation to an effective one-dimensional problem. However, within FMT one reason for its good performance stems from the fact that weighted densities are in \mathbf{r} -space convolutions of the local density with geometrical weight functions, which can be evaluated fast and accurately using fast Fourier transforms (FFTs). If we reduce the dimensionality of the problem from two dimensions to effective one dimension, weighted densities lose the property of being convolution products and the calculation becomes far less efficient and the computation time increases by orders of magnitude. For this reason we stay with a full two-dimensional system to perform our calculations, using uniformly discretized Cartesian coordinates, which do not allow for an exact representation of the hard core of the external potential. This problem can be mitigated by averaging the resulting density profile $\rho(\mathbf{r}) = \rho(r, \varphi)$ over the angle φ to obtain

$$g(r) = \frac{1}{2\pi} \int_0^{2\pi} \frac{\rho(r, \varphi)}{\rho_b} d\varphi, \quad (22)$$

where φ is the polar angle of \mathbf{r} . A few further details regarding our DFT calculations are given in Appendix B. While there are alternative numerical approaches, that allow for a computationally efficient reduction of the two dimensions to an *effective* one dimensional problem like quasi-spectral methods [27] or employing a logarithmic grid [28, 29], we decided to stick to the two dimensional implementation, because the results presented here are part of a larger project [25, 26].

In Fig. 1 we show our DFT result for the test-particle (TP) $g(r)$, calculated using FMT (red lines) for four different values of the bulk packing fraction $\eta = \pi\rho_b/4$, where we have made use of $\sigma = 1$, for a fixed shoulder range $\lambda = 3.7$. The calculations are performed at a fixed reduced temperature of $T = 0.7402$ (which corresponds to $\beta\epsilon = 1.351$). Due to the hard core of the fixed test-particle at the origin, the RDF is enforced to vanish for $r < 1$. At $r = 1$ the RDF $g(r)$ makes a jump from zero inside the core to its contact value. For $r > 1$ the RDF displays an oscillatory behaviour due to packing effects. Note, however, that

at $r = \lambda$ the interaction potential $\phi(r)$ and hence the external potential in the test-particle geometry jumps from $\epsilon > 0$ to zero and as a result $g(r = \lambda)$ changes discontinuously at this separation too. This feature is most obvious at low packing fractions, but is still clearly visible at the highest packing fraction of $\eta = 0.4$ we consider here.

We find that $g(r)$, especially at higher packing fractions, displays a complex, oscillatory behaviour, which becomes more pronounced as the packing fraction η increases. This feature is well captured by the TP results (red lines) which is not too surprising because FMT accounts for short ranged correlations due to hard cores. In order to test the quality of the test-particle results within DFT we compare them to GCMC data.

The results from the GCMC simulations are shown as black lines in Fig. 1. We find that the overall behaviour of the simulation-based $g(r)$ is captured semi-quantitatively by the TP results, with contact values of $g(r)$ and its values at the square shoulder distance $r = \lambda$ somewhat too small. It is worth mentioning that the structure of $g(r)$ for hard disks and for hard disk mixtures can be accounted for by FMT TP with much higher precision [18, 19] compared to the results presented in Fig. 1.

As already mentioned, the second approach to $g(r)$ within DFT makes use of the OZ equation (3). Instead of a closure relation, we employ the pDCF from DFT, derived from the excess free energy functional via Eq. (4). It is important to realise that for hard disks the OZ route to $g(r)$ is typically significantly less accurate than the test-particle route, while it still predicts reasonable results for the pDCF obtained from FMT.

The pDCF for the core can be calculated analytically within FMT in Fourier space, resulting in the expression for $\hat{c}_c^{(2)}(k)$ in terms of Bessel functions given in Eq. (19). The shoulder contribution to the pDCF can also be calculated analytically in Fourier space and again contains a Bessel function; see Eq. (20). While in odd dimensions ($d = 1, 3, \dots$) the Fourier transforms of the FMT weight functions can be expressed with trigonometric functions, in even dimensions ($d = 2, 4, \dots$) one finds Bessel functions instead. Once the pDCF in Fourier space is given, the OZ equation can be solved using Eq. (15) via an inverse Fourier transform. In $d = 2$ this results in an inverse Hankel transform.

In Fig. 1 we show the results from the OZ route to $g(r)$, using the pDCF obtained as blue lines. The first observation we can make is that the core condition $g(r < 1) = 0$ is violated by the OZ route. This observation has been made before for the OZ route using a pDCF obtained from an approximate excess free-energy functional, see e.g. Ref. [24]. In order

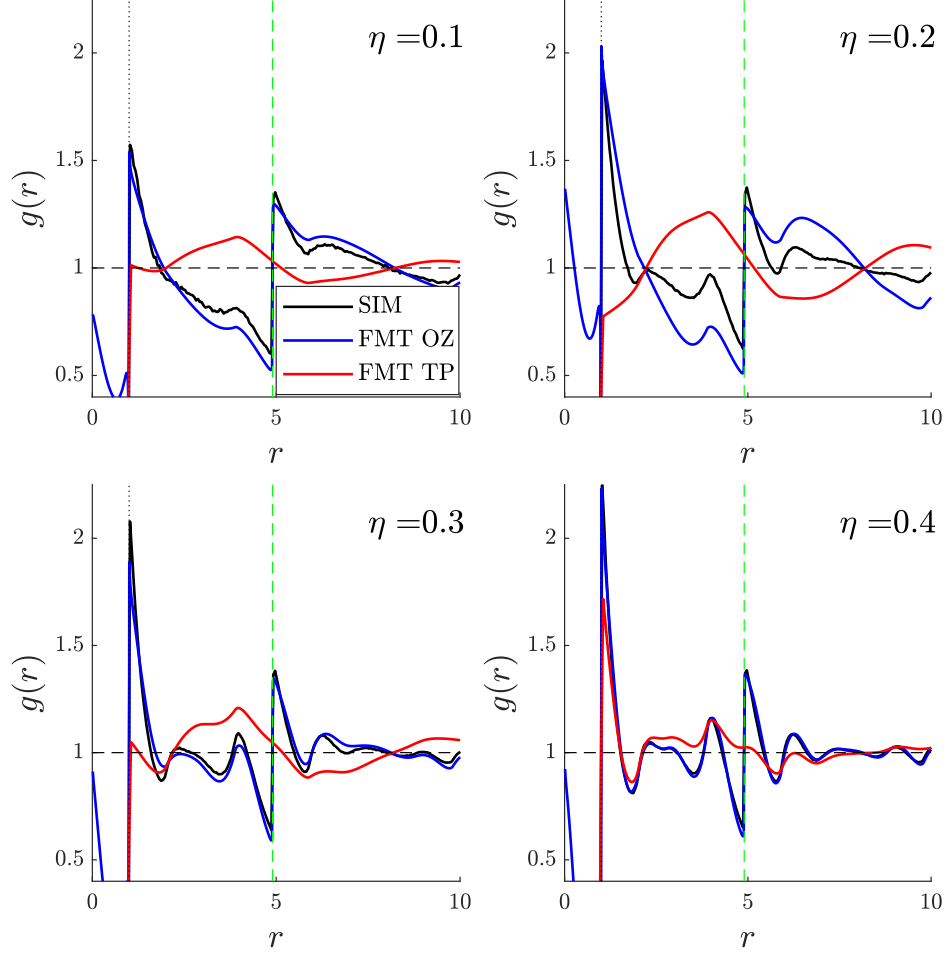


FIG. 2: RDF $g(r)$ as obtained from the Ornstein-Zernike (OZ) route (blue lines), the test-particle (TP) route (blue lines) and from GCMC simulations (black lines) for $\lambda = 4.9$ and $T = 1.2285$ and η -values as labelled. At low and intermediate densities the TP results are surprisingly bad, while the OZ results, except for the violation of the core condition, agree well with the simulation data for all densities considered here.

to avoid such a deficiency, closure relations like the Percus-Yevick closure [1, 23], enforce the core condition. We observe that the OZ results outside the core, show a reasonable agreement with the computer simulations (black lines). Furthermore, the results for $\lambda = 3.7$ using the OZ route, seem to be comparable to those from the test-particle route.

As a second example, we study the behaviour of $g(r)$ for four different values of the packing fraction η for a square-shoulder range of $\lambda = 4.9$ and a reduced temperature of $T = 1.2285$ (corresponding to $\beta\epsilon = 0.814$). We show our results for $g(r)$ in Fig. 2 and find that DFT, using the test-particle (TP) route (red lines), fails to predict a sensible $g(r)$ for low

and intermediate values of the packing fraction, i.e., for η up to $\eta = 0.3$. TP results display structures only on the size scale of the shoulder width λ and hence disagree considerably with our simulation results for $g(r)$ (black lines), which possess significant contact values and sizeable jumps at $r = \lambda$. Moreover the oscillations in the TP results are completely out of phase compared to those obtained from simulations. The TP result improves a bit at the highest value of η that we have considered in this study (i.e., $\eta = 0.4$), and starts to show the onset of the structure found in the simulations.

We observe that the OZ results, shown in Fig. 2 as blue lines agree outside of the core surprisingly well with our simulation results, especially at higher packing fractions η . Given our finding that the test-particle results for $g(r)$ for this value of λ are rather poor, this is an important and very curious result. One might expect that $g(r)$, calculated from the test-particle route is more accurate than that based on the OZ route. After all, the TP route requires only one functional derivative, while OZ route requires two. However, our results demonstrate that this is obviously not always the case.

It is clear that the main deficiency of the DFT approach is the RPA treatment of the square-shoulder potential, Eq. (13). At low densities this term, especially for large values of λ , is very strong and dominating, as it scales with the shoulder width λ like $\mathcal{F}_{\text{sh}}/\mathcal{F}_{\text{c}}^{\text{LDA/FMT}} \propto \lambda^2$. Our observations, that the structure of $g(r)$ is not captured satisfactorily for large values of λ , while FMT is able to describe the structure of the hard cores accurately [18, 19], indicates that the RPA approach is too simplistic.

IV. DISCUSSION AND SUMMARY

In this study we have considered a two dimensional system where the particles interact via a hard core interaction plus an adjacent square-shoulder potential whose range is rather long, notably up to 4.9 times the hard core diameter. We have calculated the RDF for the system via different routes. Within the DFT approach we have used the highly successful FMT for the core contributions and treated the shoulder via a standard perturbation theory approach, employing the RPA. We find some surprising outcomes for the reliability of the RDF $g(r)$. The typical route to the RDF within DFT, the test-particle route, turns out to not always the best choice, as it can give significantly less accurate predictions than the OZ route, when compared to simulation data of $g(r)$. This fact was not to be expected from

what we know from the prior literature, and raises several questions. These observations also have interesting and important implications.

We are confident that the main shortcoming of our DFT approach originates from the simple perturbative approach for the soft repulsive square-shoulder interaction, which we treat with the standard RPA ansatz, Eq. (13). This conclusion is based on the fact that for the bare hard core interaction, FMT is able to predict very accurate RDFs via the test-particle route [18, 19]. It should be mentioned that there are more sophisticated perturbation theories available [30–32] to take into account a potential tail; however, their implementation for the system at hand is definitely beyond the scope of this manuscript. A first step to improve the level of agreement between DFT- and simulation results, at least for the simple square-shoulder potential, might be to make use of the freedom we have to modify the shoulder interaction $\phi_{\text{sh}}(r)$ within the hard core region, without affecting the total interaction (which is anyhow infinite inside the core). Such an approach is known as the *optimised* random phase approximation [33], which could improve the performance of the test-particle route. Trying to improve the consistency between the OZ and the test-particle route to $g(r)$ will surely be a strategy to improve the overall accuracy of the DFT. A step in this direction might be done either by setting $\phi_{\text{sh}}(r)$ to zero inside the core or to replace it by a suitably designed function which is adjusted such that the agreement between the DFT and the simulation data is optimized. To some extent, the level of self-consistency could also be improved by adjusting the core contribution of the RPA term with the help of exact sum rules that make use of the RDF $g(r)$ employing the test-particle route [34, 35].

The work of this manuscript has even broader implications, because having an accurate theory for $c^{(2)}(r)$ is not just about getting $g(r)$ correct. There are several other important quantities that depend on $c^{(2)}(r)$, including the isothermal compressibility. Another is the static structure factor $S(k)$, and quantities derived from the pDCF $\hat{c}^{(2)}(k)$, which turn out to be accurate compared to computer simulations. This can be used to quickly and easily map out where in the phase diagram the solid phases possibly arise. The so-called dispersion relation (a quantity related simply to $\hat{c}^{(2)}(k)$), which determines the growth/decay rate of periodic density modes in the uniform liquid [36], can be employed to predict with remarkable accuracy the structure of the solid phases that form when the liquid becomes unstable [26]. In fact, by tuning the dispersion relation allows to identify pair potential parameters and state points where, for instance, quasicrystalline phases arise [26]. It is also

surprising that the DFT used here can semi-quantitatively predict phase boundaries and the wavelengths of the density modulations that determine the crystalline and quasicrystalline structures formed by core-shoulder particle systems, yet it can struggle when it comes to the seemingly simpler problem of determining the liquid-state structure. We believe all of these observations will be useful to bear in mind in future studies aimed at developing improved DFTs for core-shoulder and other systems.

ACKNOWLEDGEMENTS

The simulation results presented here were enabled via a generous allocation of CPU time by the Austrian Scientific Computing (ASC) under Project No. 71263. The authors thank Ms. Katrin Muck for her guidance related to the use of HPC. A.J.A. gratefully acknowledges support from the EPSRC under Grant No. EP/P015689/1. This research was funded in part by the Austrian Science Fund (FWF) under project no. PIN8759524 with Grant-DOI 10.55776/PIN8759524, gratefully acknowledged by GK.

APPENDIX A

We provide here further details about the OZ and test-particle routes for calculating $g(r) = 1 + h(r)$. The following arguments lean heavily on related arguments put forward in Ref. [20].

A. OZ equation with the RPA closure

The exact closure relation to the OZ equation (3) is often written as [1]

$$c^{(2)}(r) = h(r) - \ln(h(r) + 1) - \beta\phi(r) + B(r) \quad (23)$$

where $B(r)$ is termed the bridge function; $B(r)$ is in general not known exactly. The RPA-DFT approximation used here, given in Eq. (16) or Eq. (20), can be written as

$$c_{\text{RPA}}^{(2)}(r) = c_c^{(2)}(r) - \beta\phi_{\text{sh}}(r), \quad (24)$$

where $c_c^{(2)}(r)$ is the pDCF for the (purely repulsive) reference hard disk fluid, given in Eq. (17). Plugging Eq. (24) into the OZ equation (3), we obtain

$$h(r) = c_c^{(2)}(r) - \beta\phi_{\text{sh}}(r) + \rho_b \int d\mathbf{r}' h(r') c_c^{(2)}(|\mathbf{r} - \mathbf{r}'|) - \rho_b \int d\mathbf{r}' h(r') \beta\phi_{\text{sh}}(|\mathbf{r} - \mathbf{r}'|). \quad (25)$$

We now move on to derive a corresponding expression via the test-particle route.

B. The Percus test-particle route with the RPA DFT

Percus showed [11, 12] that the radial distribution function $g(r)$ is related to the density profile $\rho(\mathbf{r}) = \rho(r)$ around a fixed particle (positioned in the origin) that exerts an external potential equal to the pair potential $\phi(r)$ as: $g(r) = h(r) + 1 = \rho(r)/\rho_b$. Using DFT, $\rho(r)$ may be obtained via Eq. (2). So, minimising (5) with $V_{\text{ext}}(\mathbf{r}) = \phi(r)$, the resulting Euler-Lagrange equation reads

$$\frac{\delta\Omega[\rho]}{\delta\rho} = k_B T \ln[\Lambda^2 \rho(r)] + \frac{\delta F_c[\rho]}{\delta\rho} + \int d\mathbf{r}' \rho(r') \phi_{\text{sh}}(|\mathbf{r} - \mathbf{r}'|) + \phi(r) - \mu = 0. \quad (26)$$

Far from the test particle, at $r \rightarrow \infty$ the density $\rho(r) \rightarrow \rho_b$ and $\phi(r) = 0$. In this limit, Eq. (26) gives

$$k_B T \ln[\Lambda^2 \rho_b] + \frac{\delta F_c[\rho]}{\delta\rho} \Big|_{\rho_b} + \rho_b \int d\mathbf{r} \phi_{\text{sh}}(r) - \mu = 0. \quad (27)$$

If we subtract Eq. (27) from Eq. (26), we obtain:

$$0 = k_B T \ln\left(\frac{\rho(r)}{\rho_b}\right) + \frac{\delta F_c[\rho]}{\delta\rho} - \frac{\delta F_c[\rho]}{\delta\rho} \Big|_{\rho_b} + \int d\mathbf{r}' (\rho(r') - \rho_b) \phi_{\text{sh}}(|\mathbf{r} - \mathbf{r}'|) + \phi(r). \quad (28)$$

Multiplying through by $(-\beta)$ and adding $(\rho(r) - \rho_b)/\rho_b$ to both sides, together with making use of the following functional Taylor expansion about the bulk density:

$$\frac{\delta F_c[\rho]}{\delta\rho} = \frac{\delta F_c[\rho]}{\delta\rho} \Big|_{\rho_b} + \int d\mathbf{r}' (\rho(\mathbf{r}') - \rho_b) \frac{\delta^2 F_c[\rho]}{\delta\rho(\mathbf{r}) \delta\rho(\mathbf{r}')} \Big|_{\rho_b} + H_c[\rho(\mathbf{r})], \quad (29)$$

where $H_c[\rho(\mathbf{r})]$ denotes all higher order terms which are $\sim \mathcal{O}([\rho - \rho_b]^2)$ and higher, we obtain:

$$\begin{aligned} \frac{(\rho(r) - \rho_b)}{\rho_b} &= \frac{(\rho(r) - \rho_b)}{\rho_b} - \ln\left(\frac{\rho(r)}{\rho_b}\right) - \beta\phi(r) + \rho_b \int d\mathbf{r}' \frac{(\rho(r') - \rho_b)}{\rho_b} \left[\frac{-\beta\delta^2 F_c[\rho]}{\delta\rho(\mathbf{r}) \delta\rho(\mathbf{r}')} \Big|_{\rho_b} \right] \\ &\quad - \beta H_c[\rho(r)] + \rho_b \int d\mathbf{r}' \frac{(\rho(r') - \rho_b)}{\rho_b} \phi_{\text{sh}}(|\mathbf{r} - \mathbf{r}'|). \end{aligned} \quad (30)$$

Now, recalling Eq. (4), we therefore have that

$$c_c^{(2)}(|\mathbf{r} - \mathbf{r}'|) = \frac{-\beta\delta^2 F_c[\rho]}{\delta\rho(\mathbf{r}) \delta\rho(\mathbf{r}')} \Big|_{\rho_b}, \quad (31)$$

so that Eq. (30) becomes

$$\begin{aligned}
h(r) = & h(r) - \ln(h(r) + 1) - \beta\phi(r) - \beta H_c[\rho_b g(r)] \\
& + \rho_b \int d\mathbf{r}' h(r') c_c^{(2)}(|\mathbf{r} - \mathbf{r}'|) - \rho_b \int d\mathbf{r}' h(r') \beta\phi_{\text{sh}}(|\mathbf{r} - \mathbf{r}'|).
\end{aligned}
\tag{32}$$

If $F_c[\rho]$ were exact, then $-\beta H_c[\rho_b g(r)]$ would be the bridge-function $B_c(r)$ of the reference hard disk fluid [20]. Thus, comparing the first four terms on the right hand side of Eq. (32) with the right hand side of Eq. (23), we see that these four terms together correspond to an approximation for $c^{(2)}(r)$ that is neither the exact result (23), nor the RPA approximation (24). This close similarity to the exact expression in Eq. (23), with the only difference being the approximation effectively made for the bridge function $B(r)$, formed the basis of the arguments in Ref. [20] that mean-field DFT is often better than one might expect. It is also one reason why the test-particle route to $g(r)$ is generally expected to be superior to the OZ route.

However, the present work contradicts this general expectation [20, 24, 37]. In the present case, from comparing Eq. (25) with Eq. (32), we see that all the differences between the two approaches originate not from the two final convolution terms, but instead from the subtle interplay between the other terms. We conjecture that the non-linear terms in Eq. (32) must be playing a crucial role in this delicate balance, amplifying and damping features in a very different way to the corresponding terms in the linear Eq. (25).

APPENDIX B

The DFT calculations were performed using a code written by the authors that is available online via [38], using distributed memory parallelization of the FFT via the mpi4py-fft package [39]. The RDFs are obtained using Picard iteration; for details on the numerical implementation we refer to previous work using the same software [25]. The test-particle located at $(x = 0, y = 0)$ is included via the shoulder part of the potential in Eq. (14), treated explicitly as external potential term in the minimized free energy, while the hard core repulsion is enforced by setting the density within the core $\rho(r < \sigma) \equiv 0$, at every iteration step. The calculations are carried out in square boxes of size $L_x = L_y = 50\sigma$, discretized on $N_x = N_y = 2048$ grid points using periodic boundary conditions. The resulting density profiles are then angular-averaged according to Eq. (22) using 500 evenly spaced radial bins.

To verify that neither the resolution nor the boundary conditions are affecting the described features of $g(r)$, we performed DFT calculations for $\lambda = 4.9$ at $\eta = 0.4$ varying both box size and number of grid points and found no significant effect of both computational parameters on the resulting $g(r)$. A calculation was considered converged, if the cumulative squared error between the densities of consecutive steps in the Picard iteration fell below 10^{-13} .

The $g(r)$ via the OZ route are calculated from the structure factor $S(k) = [1 - \rho\hat{c}^{(2)}(k)]^{-1}$ (see Eq. (16)) by numerical integration of the inverse Hankel transform

$$g(r) = 1 + \frac{1}{2\pi\rho} \int_0^\infty (S(k) - 1)kJ_0(kr)dk. \quad (33)$$

The radius in Fourier space $k \in (0.025, 250)$ was discretized uniformly with grid spacing $dk = 0.025$. The numerical integration of the above integral was then performed for the uniformly spaced real space radii $r \in (\frac{2\pi}{250}, \frac{2\pi}{dk} = 2\pi \cdot 40)$.

BIBLIOGRAPHY

- [1] J. P. Hansen and I. R. McDonald, *Theory of Simple Liquids* (Academic Press, Oxford, 2013).
- [2] R. Evans, R. J. F. Leote de Carvalho, J. R. Henderson, and D. C. Hoyle, Asymptotic decay of correlations in liquids and their mixtures, *J. Chem. Phys.* **100**, 591 (1994).
- [3] N. D. Mermin, Thermal properties of the inhomogeneous electron gas, *Phys. Rev.* **137**, A1441 (1965).
- [4] R. Evans, The nature of the liquid-vapour interface and other topics in the statistical mechanics of non-uniform, classical fluids, *Adv. Phys.* **28**, 143 (1979).
- [5] L. S. Ornstein and F. Zernike, Accidental deviations of density and opalescence at the critical point of a single substance, Koninklijke Nederlandse Akademie van Wetenschappen Proceedings Series B Physical Sciences **17**, 793 (1914).
- [6] N. Metropolis, A. W. Rosenbluth, M. N. Rosenbluth, A. H. Teller, and E. Teller, Equation of state calculations by fast computing machines, *J. Chem. Phys.* **21**, 1087 (1953).
- [7] P. Tarazona and R. Evans, A simple density functional theory for inhomogeneous liquids, *Mol. Phys.* **52**, 847 (1984).
- [8] P. Tarazona, Free-energy density functional for hard spheres, *Phys. Rev. A* **31**, 2672 (1985).
- [9] Y. Rosenfeld, Free-energy model for the inhomogeneous hard-sphere fluid mixture and density-functional theory of freezing, *Phys. Rev. Lett.* **63**, 980 (1989).

- [10] R. Roth, Fundamental measure theory for hard-sphere mixtures: a review, *J. Phys.: Condens. Matter* **22**, 063102 (2010).
- [11] J. K. Percus, Equilibrium state of a classical fluid of hard rods in an external field, *J. Stat. Phys.* **15** (1976).
- [12] T. K. Vanderlick, H. T. Davis, and J. K. Percus, The statistical mechanics of inhomogeneous hard rod mixtures, *J. Chem. Phys.* **91**, 7136 (1989).
- [13] R. Roth, R. Evans, A. Lang, and G. Kahl, Fundamental measure theory for hard-sphere mixtures revisited: the White Bear version, *J. Phys. Condens. Matter* **14**, 12063 (2002).
- [14] Y.-X. Yu and J. Wu, Structures of hard-sphere fluids from a modified fundamental-measure theory, *J. Chem. Phys.* **117**, 10156 (2002).
- [15] H. Hansen-Goos and R. Roth, Density functional theory for hard-sphere mixtures: the White Bear version mark II, *J. Phys. Condens. Matter* **18**, 8413–8425 (2006).
- [16] J. F. Lutsko, Explicitly stable fundamental-measure-theory models for classical density functional theory, *Phys. Rev. E* **102**, 062137 (2020).
- [17] Y. Rosenfeld, Free-energy model for the inhomogeneous hard-sphere fluid in d dimensions: Structure factors for the hard-disk ($d=2$) mixtures in simple explicit form, *Phys. Rev. A* **42**, 5978 (1990).
- [18] R. Roth, K. Mecke, and M. Oettel, Fundamental measure theory for hard disks: Fluid and solid, *J. Chem. Phys.* **136**, 081101 (2012).
- [19] A. L. Thorneywork, S. K. Schnyder, D. G. Aarts, J. Horbach, R. Roth, and R. P. Dullens, Structure factors in a two-dimensional binary colloidal hard sphere system, *Mol. Phys.* **116**, 3245 (2018).
- [20] A. J. Archer, B. Chacko, and R. Evans, The standard mean-field treatment of inter-particle attraction in classical DFT is better than one might expect, *J. Chem. Phys.* **147**, 034501 (2017).
- [21] J. K. Percus, Approximation methods in classical statistical mechanics, *Phys. Rev. Lett.* **8**, 462 (1962).
- [22] J. K. Percus, The equilibrium theory of classical fluids, in *Frontiers in Physics: Lecture note and reprint series, A*, edited by H. L. Frisch and J. L. Lebowitz (W.A. Benjamin, 1964).
- [23] J. K. Percus and G. J. Yevick, Analysis of classical statistical mechanics by means of collective coordinates, *Phys. Rev.* **110**, 1 (1958).

- [24] M. Schmidt, Density functional for additive mixtures, *Phys. Rev. E* **62**, 3799 (2000).
- [25] M. Wassermair, G. Kahl, R. Roth, and A. J. Archer, Fingerprints of ordered self-assembled structures in the liquid phase of a hard-core, square-shoulder system, *J. Chem. Phys.* **161**, 124503 (2024).
- [26] M. Wassermair, G. Kahl, R. Roth, and A. J. Archer, Navigating complex soft-matter phase diagrams, *Phys. Rev. Lett.* (2026).
- [27] A. Nold, B. D. Goddard, P. Yatsyshin, N. Savva, and S. Kalliadasis, Pseudospectral methods for density functional theory in bounded and unbounded domains, *Journal of Computational Physics* **334**, 639 (2017).
- [28] A. J. S. Hamilton, Uncorrelated modes of the non-linear power spectrum, *Mon. Not. R. Astron. Soc.* **312**, 257 (2000).
- [29] V. Boğan, F. Pesth, T. Schilling, and M. Oettel, Hard-sphere fluids in annular wedges: Density distributions and depletion potentials, *Phys. Rev. E* **79**, 061402 (2009).
- [30] J. A. Barker and D. Henderson, What is "liquid"? understanding the states of matter, *Rev. Mod. Phys.* **48**, 587 (1976).
- [31] J. D. Weeks, D. Chandler, and H. C. Andersen, Role of repulsive forces in determining the equilibrium structure of simple liquids, *J. Chem. Phys.* **54**, 5237 (1971).
- [32] S. M. Tschopp, H. D. Vuijk, A. Sharma, and J. M. Brader, Mean-field theory of inhomogeneous fluids, *Phys. Rev. E* **102**, 042140 (2020).
- [33] G. Kahl and J. Hafner, Optimized random-phase approximation for the structure of expanded fluid rubidium, *Phys. Rev. A* **29**, 3310 (1984).
- [34] M. Gül, R. Roth, and R. Evans, Using test particle sum rules to construct accurate functionals in classical density functional theory, *Phys. Rev. E* **110**, 064115 (2024).
- [35] M. Gül, R. Roth, and R. Evans, Using test particle sum rules to improve approximations in classical density functional theory: White-Bear and White-Bear mark II versions of the Lutsko functional, *Phys. Rev. E* **113**, 034104 (2026).
- [36] A. J. Archer and R. Evans, Dynamical density functional theory and its application to spinodal decomposition, *J. Chem. Phys.* **121**, 4246 (2004).
- [37] P. Hopkins and M. Schmidt, Radial distribution functions of non-additive hard sphere mixtures via Percus' test particle route, *J. Phys.: Condens. Matter* **23**, 325104 (2011).
- [38] <https://github.com/watermair/PDFT>, (2026).

- [39] L. Dalcin, M. Mortensen, and D. E. Keyes, Fast parallel multidimensional FFT using advanced MPI, *J. Parallel Distrib. Comput.* **128**, 137 (2019).